RESEARCH ARTICLE

Effects of episodic rainfall on a subterranean estuary

Xiayang Yu[1], Pei Xin[1] , Chunhui Lu[1] , Clare Robinson[2], Ling Li[3] , and D. A. Barry[4]

[1]State Key Laboratory of Hydrology-Water Resources and Hydraulic Engineering, Hohai University, Nanjing, China, [2]Department of Civil and Environmental Engineering, Western University, London, Ontario, Canada, [3]School of Civil Engineering, The University of Queensland, Queensland, Australia, [4]Laboratoire de technologie écologique (ECOL), Institut d'ingénierie de l'environnement (IIE), Faculté de l'environnement naturel, architectural et construit (ENAC), Ecole Polytechnique Fédérale de Lausanne (EPFL), Lausanne, Switzerland

Abstract Numerical simulations were conducted to examine the effect of episodic rainfall on nearshore groundwater dynamics in a tidally influenced unconfined coastal aquifer, with a focus on both long-term (yearly) and short-term (daily) behavior of submarine groundwater discharge (SGD) and seawater intrusion (SWI). The results showed nonlinear interactions among the processes driven by rainfall, tides, and density gradients. Rainfall-induced infiltration increased the yearly averaged fresh groundwater discharge to the ocean but reduced the extents of the saltwater wedge and upper saline plume as well as the total rate of seawater circulation through both zones. Overall, the net effect of the interactions led to an increase of the SGD. The nearshore groundwater responded to individual rainfall events in a delayed and cumulative fashion, as evident in the variations of daily averaged SGD and salt stored in the saltwater wedge (quantifying the extent of SWI). A generalized linear model (GLM) along with a Gamma distribution function was developed to describe the delayed and prolonged effect of rainfall events on short-term groundwater behavior. This model validated with results of daily averaged SGD and SWI from the simulations of groundwater and solute transport using independent rainfall data sets, performed well in predicting the behavior of the nearshore groundwater system under the combined influence of episodic rainfall, tides, and density gradients. The findings and developed GLM form a basis for evaluating and predicting SGD, SWI, and associated mass fluxes from unconfined coastal aquifers under natural conditions, including episodic rainfall.

1. Introduction

The freshwater-saltwater mixing zone in a coastal aquifer, called subterranean estuary, plays an important role in controlling chemical fluxes from the aquifer to ocean [*Burnett et al.*, 2006; *Moore*, 1999, 2010; *Robinson et al.*, 2009; *Santos et al.*, 2012]. In this zone, submarine groundwater discharge (SGD) and seawater intrusion (SWI) are two complementary processes [*Moore*, 2010; *Werner et al.*, 2013], with the former covering all the water effluxes across the land-ocean interface and the latter linked to the extent of intruded saltwater in a coastal aquifer. Recent studies suggested that chemical fluxes associated with SGD can be comparable to riverine chemical inputs into the sea [*Kwon et al.*, 2014; *Moore*, 1996; *Rodellas et al.*, 2015; *Wang et al.*, 2015]. SGD and SWI have been studied intensively in recent decades due to their significant impacts on coastal environments and water quality in coastal aquifers [*Bakhtyar et al.*, 2012, 2013; *Brovelli et al.*, 2007; *Lu et al.*, 2015; *Michael et al.*, 2013; *Moore*, 2010; *Santos et al.*, 2012; *Wang et al.*, 2015; *Werner et al.*, 2013].

Terrestrial groundwater discharge, density-driven flow, tides, and waves are major driving forces affecting SGD and SWI in coastal aquifers (Figure 1) [*Burnett et al.*, 2006; *Heiss and Michael*, 2014; *Li et al.*, 1999; *Michael et al.*, 2016; *Moore et al.*, 2008; *Taniguchi et al.*, 2002; *Xin et al.*, 2010]. In early work, it was assumed that SGD could be estimated based on a summation of fluxes driven by these forces independently [*Burnett et al.*, 2006; *Li et al.*, 1999; *Taniguchi et al.*, 2002], i.e.,

$$\text{SGD} \ = \ Q_f + Q_c = Q_f + Q_d + Q_t + Q_w \tag{1}$$

where Q_f and Q_c are the inland freshwater input and total circulating seawater flux, respectively; and Q_c is given by a linear combination of the density-driven flow (Q_d), tidally driven flow (Q_t), and wave-induced flow (Q_w).

In the presence of a seaward hydraulic gradient, fresh terrestrial groundwater flows toward, and discharges into the coastal sea. In the absence of tides and waves on the seaward side, fresh groundwater flows
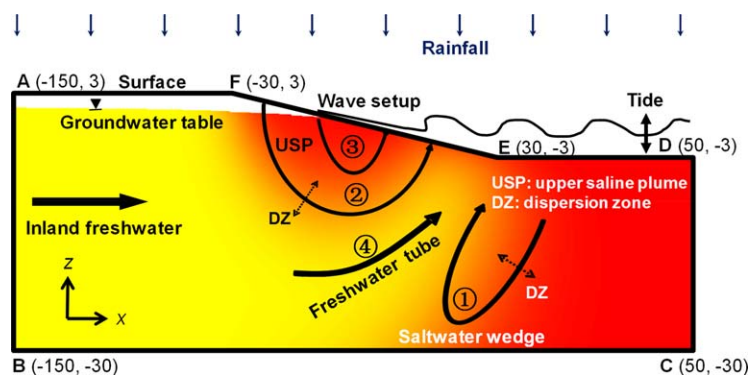
Figure 1. Conceptual diagram of an unconfined near-shore aquifer (subterranean estuary) including major flow processes: (1) density-driven recirculation, (2) tide-induced recirculation, (3) recirculation driven by wave setup, and (4) terrestrial groundwater discharge including freshwater influx generated by rainfall infiltration. The colors represent the salinity (red for seawater and yellow for freshwater). Boundary ABCDEF is the model domain. The *x-z* coordinate origin was set at the mean shoreline. The coordinates of the domain reference points for Cases 1–6 are given in the unit of m. The upper boundary (AF) was extended upward by 2 m in Case 7 and the left boundary (AB) was extended landward by 50 m in Case 8. Note that wave forcing is not considered in the present study.

above the denser seawater associated with the saltwater wedge (SW). Convective circulation of seawater through the SW is caused by the density-gradient and affected by hydrodynamic dispersion along the freshwater-saltwater transition zone of the SW [*Cooper*, 1959] (Figure 1). The extent of the intruding saltwater wedge generally increases with decreasing fresh groundwater discharge (Q_f) [*Glover*, 1959; *Smith*, 2004; *Werner et al.*, 2013].

Most coastlines worldwide are exposed to tides. The effect of tides on subterranean estuaries has been studied intensively over the last 10 years [*Anschutz et al.*, 2009; *Heiss and Michael*, 2014; *Kuan et al.*, 2012; *Li et al.*, 2008; *Mao et al.*, 2006; *Robinson et al.*, 2006, 2007a, 2007b, 2009; *Wilson et al.*, 2015; *Zhang et al.*, 2016]. Tidal fluctuations drive seawater circulations in shallow intertidal aquifers, alter the salt distribution and, under certain conditions, lead to the formation of an upper saline plume (USP) (Figure 1) [*Evans and Wilson*, 2016; *Heiss and Michael*, 2014; *Robinson et al.*, 2006, 2007a]. Fresh groundwater discharges through a "tube" bounded by the USP and lower SW [*Boufadel*, 2000; *Robinson et al.*, 2007a]. The tide-induced seawater circulations can contribute significantly to the total SGD [*Burnett et al.*, 2006; *Li et al.*, 1999; *Robinson et al.*, 2007a] and limit the extent of SWI [*Kuan et al.*, 2012].

Waves are another important forcing factor for a nearshore subterranean estuary. The effects of waves are mainly manifested in wave setup, an onshore upward tilt in the mean sea level that drives a seawater circulation similar to that induced by tides [*Bakhtyar et al.*, 2013; *Geng et al.*, 2014; *Li and Barry*, 2000; *Longuet-Higgins*, 1983; *Robinson et al.*, 2014; *Xin et al.*, 2010]. This circulation also increases the total SGD and inhibits the SWI. In contrast to tides, which have well-defined principal frequencies (e.g., spring-neap tides with semidiurnal solar and lunar frequencies), waves are highly random with the height and period varying irregularly [*Heiss et al.*, 2015; *Xin et al.*, 2014]. This leads to dynamic and irregular variations of SGD, SWI, and USP at various temporal scales [*Robinson et al.*, 2014; *Xin et al.*, 2014].

Evaporation and rainfall lead to net water loss and gain for the aquifer, which affect groundwater discharge to the ocean. The effect of evaporation on nearshore groundwater slightly reduces the total SGD but increases considerably the pore water salinity in the intertidal zone [*Geng and Boufadel*, 2015; *Geng et al.*, 2016]. The rainfall effect, however, has not been investigated directly. Rainfall induces water infiltration that increases the aquifer recharge and raises the water table [*Evans and Wilson*, 2017; *Heiss and Michael*, 2014; *Jun et al.*, 2013; *Li et al.*, 2009]. This would affect the SGD and SWI processes in the nearshore zone. A particular question is how rainfall interacts with other forcing factors, including tides and density gradients. Interactions among different forces on the nearshore groundwater are nonlinear and requires careful consideration in applying equation (1) for estimating the total SGD [*King*, 2012; *Sawyer et al.*, 2013; *Xin et al.*, 2010, 2014, 2015]. Each term in the equation cannot be treated as being solely dependent on a particular forcing factor but instead are functions of all the interacting forces.

The effect of rainfall on nearshore groundwater is likely to be long-lasting and cumulative, and is expected to result in hysteretic groundwater response, i.e., dependence of the present groundwater behavior on past rainfall events. *Xin et al.* [2014] examined the hysteresis of SGD driven by irregular waves and developed a hysteretic model based on functional data analysis [*Ramsay and Silverman*, 2005]. In the model, the effects of past wave conditions on SGD were assumed to vary over a continuum and were described by a continuous and smooth function (Gamma distribution function). Given its episodic nature, it is unclear whether the

effect of rainfall on SGD and SWI processes in the nearshore aquifer can be described similarly by a hysteretic model.

This study aims to examine the impact of rainfall based on numerical simulations with year-long data of episodic rainfall generated randomly to drive the nearshore groundwater flow and (salt) solute processes that are also affected by tides and density gradients. The analysis of the simulation results focuses on both long-term and short-term nearshore groundwater responses with respect to yearly and daily averaged SGD and SWI. The yearly averaged SGD and SWI are analyzed to reveal the interactions of rainfall, tide, and density gradients. The variations of daily averaged quantities are linked to rainfall events through functional data analysis with the intention to develop a predictive, hysteretic model of SGD and SWI under episodic rainfall conditions.

2. Numerical Model and Simulations

The 2-D model simulates a vertical cross-shore section of a nearshore unconfined aquifer with a setup similar to those adopted in previous studies (Figure 1) [*Geng and Boufadel*, 2015; *Kuan et al.*, 2012; *Liu et al.*, 2016; *Robinson et al.*, 2007a; *Xin et al.*, 2010, 2014]. The model domain and parameter values were based on the conditions of a field site on the west coast of Moreton Island, Australia [*Robinson et al.*, 2006]. At the site, oceanic oscillations are dominated by semidiurnal tides. The aquifer was assumed to be homogeneous and isotropic [*Robinson et al.*, 2006].

Variably saturated and density-dependent pore water flow coupled with salt transport in the aquifer was simulated using SUTRA [*Voss and Provost*, 2008] under various forcing conditions including rainfall, tides, and density gradients.

In SUTRA, pore water flow is described by the Richards equation [*Richards*, 1931] with the relative hydraulic conductivity and soil saturation calculated using the *van-Genuchten* [1980] formulas (details in *Xin et al.* [2010]). The model parameter values used in the simulations were representative of a permeable sandy coastal aquifer [*Robinson et al.*, 2006] with hydraulic conductivity $K_s = 10$ m/d, porosity $\phi = 0.45$, longitudinal dispersivity $\alpha_L = 0.5$ m, and transverse dispersivity $\alpha_T = 0.05$ m. The residual soil water saturation S_{Wres} was set to 0.1 while the shape parameters α and n were set to 14.5 m^{-1} and 2.68, respectively, for the *van-Genuchten* [1980] formulas [*Carsel and Parrish*, 1988]. This model setup was also used previously by *Xin et al.* [2010].

The occurrence, duration, and intensity of rainfall over a year, R [LT^{-1}], were determined by a Markov-chain Monte-Carlo simulator [*Morris*, 1995] (Figure 2), in which the probability of dry weather following an hour of rain was set to 10% and the probability of rain following an hour of dry weather to 1%. The rainfall intensity followed a normal distribution with a mean intensity of 2 mm/h and standard variation of 0.5 mm/h. The annual rainfall of the generated random rainfall series was around 1.6 m occurring over approximately 80 events. The rainfall pattern was assumed to repeat on an annual basis and hence the generated year-long rainfall data were applied to all simulation years.

Rainfall-induced vertical infiltration was simulated as water influx across the aquifer surface including the exposed beach section. Based on the pore water pressur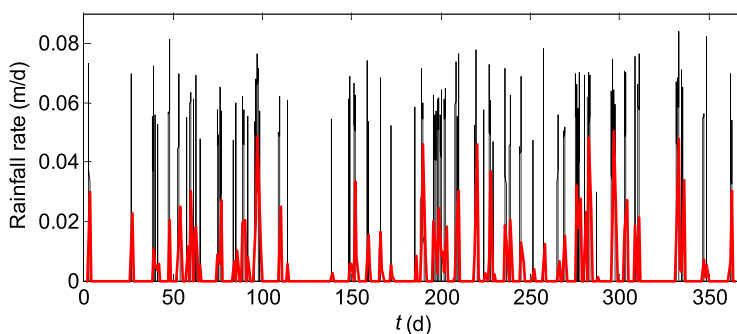e (P) at the node immediately below the aquifer surface, the local maximum infiltration rate under the surface ponding condition of zero water depth was calculated as $I_{max} = -K_s[1 - P/(\rho g \Delta z)]$, where Δz is the vertical grid size, ρ is the fluid density, and g is the gravitational acceleration. The rainfall infiltration rate (RI) was then determined according to $RI = \min(R, I_{max})$. It should be noted that a sandy coastal unconfined aquifer was considered in the

Figure 2. Annual rainfall time series used in the simulations. The red line indicates the daily averaged results.

Table 1. Simulated Cases with Model Setup and Key Results of Long-Term SGD and Salt Mass[a]

| Case | Model Domain | Tide | Rainfall | | Per Unit Width Influx (m³/m/d) | | | | Per Unit Width Efflux (SGD) (m³/m/d) | Salt Mass Stored in Per Unit Width Aquifer (kg/m) | |
					Q_f	Q_t	Q_d	Q_r		Saltwater Wedge	Upper Saline Plume
1	Figure 1	Without	Without	NA	2.10	NA	0.16	NA	2.26	32,499	NA
2	Figure 1	Without	With	Top	2.10	NA	0.17	0.62	2.89	26,583	NA
3	Figure 1	Without	With[b]	Left	2.10 + 0.62[b]	NA	0.16	NA	2.88	26,867	NA
4	Figure 1	With	Without	NA	2.10	2.56	0.56	NA	5.22	16,801	3498
5	Figure 1	With	With	Top	2.10	2.21	0.58	0.61	5.50	15,255	2485
6	Figure 1	With	With[b]	Left	2.10 + 0.62[b]	2.21	0.58	NA	5.51	15,352	2526
7	AF in Figure 1 was extended upward by 2 m	With	With	Top	2.10	2.14	0.58	0.61	5.43	15,569	2560
8	AB in Figure 1 was extended landward by 50 m	With	With[b]	Left	2.10 + 0.62[b]	2.21	0.58	NA	5.51	15,343	2504

[a]All the results are yearly averaged. Q_f is the inland freshwater input, Q_t is the circulating flux induced by tide, Q_d is the density-driven flux, and Q_r is the rainfall infiltration.
[b]The rainfall infiltration was considered as the inland freshwater input across the inland boundary. NA means not applicable.

simulations. The soil under the aquifer platform (AF in Figure 1) was largely unsaturated, with an infiltration capacity larger than the maximum rainfall rate. Thus, infiltration-excess runoff did not occur. On the sloping beach (EF in Figure 1), tides induced a moving boundary condition, which led to increase and decrease of the recharge area (in width) on falling and rising tides, respectively (more details in section 3.1).

The details of the model setup and boundary conditions for all the simulations are given in Table 1. To explore how rainfall combines with tides and density gradients to influence the nearshore groundwater dynamics, simulations were conducted with and without rainfall, and under both nontidal (static sea level, Cases 1–3) and tidal (sea level oscillating with the semidiurnal tide, Cases 4–6) conditions. The inland freshwater influx was set to 2.1 m³/m/d (per unit width aquifer) for most simulation cases. In two reference cases without rainfall (Cases 3 and 6), fluxes matching the total rainfall-induced daily averaged infiltration rates were added uniformly to the landward boundary to evaluate the effect of vertical recharge versus increased inland groundwater influx. Additional two simulations (Cases 7 and 8) were conducted to examine the effect of increased model domain sizes in both vertical and cross-shore directions, i.e., the upper boundary (AF) was extended upward by 2 m in Case 7 (note that the beach, EF, was also extended to fix the beach slope) and the left boundary (AB) was extended landward by 50 m in Case 8 (see *Xin et al.* [2010] for the detailed setup of the tide-induced moving boundary).

3. Results and Analysis

3.1. Long-Term Rainfall Effect Based on Yearly Averaged Results

The simulations were run with no rainfall included for 5 years to reach a steady (for Case 1) or quasi steady (periodic) state (for Case 4) with respect to both hydraulic heads and salinity distribution. These simulations produced similar results (Figures 3a and 3c) to those of *Robinson et al.* [2007a] and *Xin et al.* [2010], in particular, changes of the salinity distribution due to the influence of tides (Figure 3c for Case 4 versus Figure 3a for Case 1). These results served as a model verification. Tide-induced recirculation led to the formation of an USP in the intertidal zone. The freshwater-saltwater mixing zone expanded, while the extent of the SWI decreased (i.e., the toe of the SW retreated from $x = -40$ to -10 m, $z = -30$ m).

The simulations were subsequently run for another 5 years with the year-long rainfall data applied repeatedly for each year. The groundwater system reached a new quasi steady state with invariant yearly averaged flux (SGD) and salt distributions. In the nontidal case (Case 2), rainfall produced an additional freshwater influx of 0.62 m³/m/d (per unit width aquifer) to the aquifer (through the upper boundary). This was the same as the total rainfall rate on the exposed aquifer surface (0.62 m³/m/d, 150 m in the cross-shore direction), indicating strong infiltration capacity during the rainfall events. As expected, the rainfall-induced infiltration increased the freshwater discharge to the ocean, which in turn reduced the extent of SWI in the aquifer—the toe of the SW retreated from $x = -40$ m in Case 1 to -30 m in Case 2 (Figure 3b versus 3a, $z = -30$ m).
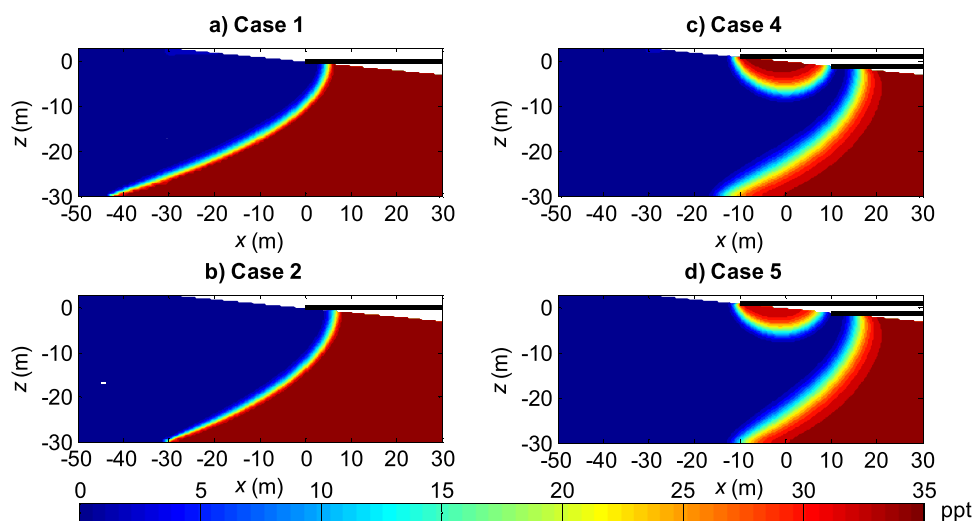
Figure 3. Yearly averaged salinity distributions in the subterranean estuary. Cases are indicated in the figure titles. The left hand side plots are for the nontidal cases, in which the black lines indicate the static sea level. The right side plots are for the tidal cases, in which the black lines indicate the tidal range. The results for Cases 3 and 6 were, respectively, similar to those for Cases 2 and 4 (see supporting information Figure S1).

In the tidal case (Case 5), rainfall produced a freshwater influx to the aquifer at the annual average rate of 0.61 m^3/m/d, slightly less than that for the nontidal case (Case 2) due to the reduced infiltration capacity in the intertidal zone. This again increased the freshwater discharge to the ocean. As a result, the USP contracted and the SW retreated as evident in the comparison with Case 4 with no rainfall (Figure 3d versus 3c). We calculated the salt mass stored in, respectively, the USP (SM_{USP}) and SW (SM_{SW}, note that only the area of $x \leq 20$ m was considered as seawater occupied the area for $x > 20$ m) (Table 1). The yearly averaged SM_{USP} decreased from 3498 kg/m in Case 4 to 2485 kg/m in Case 5, due to contraction of the USP. This is consistent with the results of *Robinson et al.* [2007a], which demonstrated that the size of the USP is controlled by the magnitude of tidal forcing relative to the fresh groundwater discharge rate. The retreat of the SW led to a reduction of SM_{SW} from 16,801 (Case 4) to 15,255 (Case 5) kg/m. This reduction, 1546 kg/m, was significantly less than that under the nontidal condition, i.e., the difference between Case 1 and Case 2 (5916 kg/m).

As expected, rainfall infiltration modified the water fluxes across the aquifer-ocean interface (Figure 4). In the nontidal case, rainfall infiltration increased the total SGD from 2.26 (Case 1) to 2.89 (Case 2) m^3/m/d across a slightly expanded water efflux zone (Table 1 and Figure 4a). The increase of SGD was largely due to the additional freshwater influx/discharge induced by rainfall and also a slightly larger flux of circulating seawater through the SW driven by density gradients (0.17 m^3/m/d in Case 2 compared with 0.16 m^3/m/d in Case 1). The increase of the seawater circulation rate was caused by intensified freshwater-seawater mixing in the mixing zone of the SW due to increased freshwater discharge [*Smith*, 2004].

Tides induced significant seawater circulation at a rate of 2.56 m^3/m/d (Q_t) in the intertidal zone with influx occurring between the high tide level and the mean sea level ($-10 \leq x \leq 0$ m, Figure 4b), as shown by Case 4 in comparison with Case 1. The tidal effect also produced an increased rate of seawater circulation through the SW (0.56 m^3/m/d compared with 0.16 m^3/m/d in Case 1). As discussed above, rainfall generated an additional freshwater influx of 0.61 m^3/m/d to the aquifer, which increased the total freshwater discharge but reduced the extents of the USP and SW. The rainfall effect also resulted in a reduction in the tidal seawater circulation (Q_t), similar to that of Case 4. However, the seawater circulation through SW driven by density gradients (Q_d) was enhanced slightly (increased from 0.56 m^3/m/d in Case 4 to 0.58 m^3/m/d in Case 5), similar to the nontidal case (Case 2). The net effect of rainfall led to an increase of SGD from 5.22 m^3/m/d in Case 4 to 5.50 m^3/m/d in Case 5. Despite an additional freshwater influx of 0.61 m^3/m/d induced by rainfall, the SGD increased by only less than half of that amount (0.28 m^3/m/d).

These results demonstrate strong interactions among the forces in controlling the nearshore groundwater processes: rainfall-induced freshwater discharge and seawater circulations in the USP and SW driven by
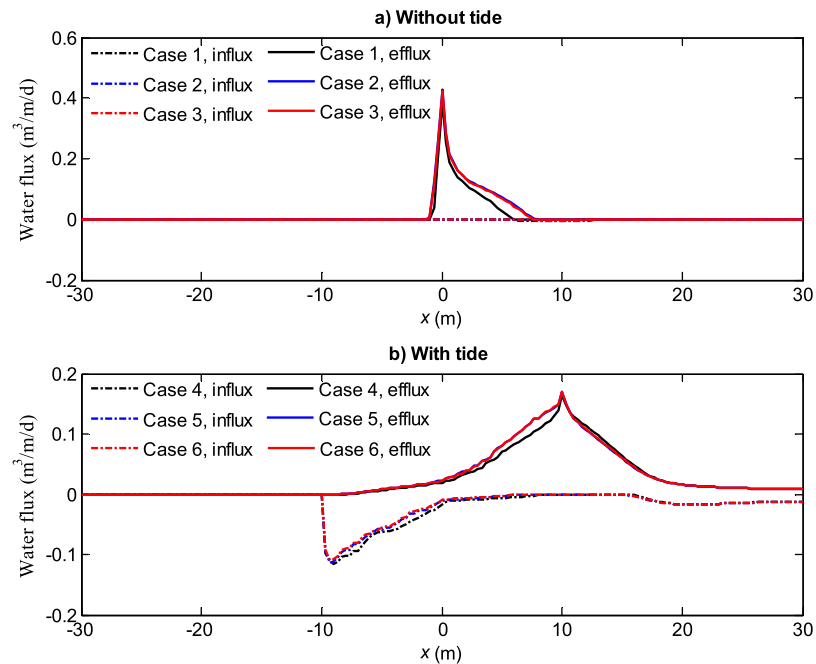
Figure 4. Yearly averaged water influx and efflux rates per-unit-area along the aquifer-ocean interface. Figure 4a is for the nontidal cases. The lines for the influx of Cases 1, 2, and 3 overlap as do the lines for the efflux of Cases 2 and 3. Figure 4b is for the tidal cases. Note that the influx excluded the rainfall infiltration. The lines for the influx and efflux of Cases 5 and 6 overlap.

tides and density gradients, respectively. Such interactions must be considered in estimating SGD, particularly when equation (1) is used. The coupling effects of different forces need to be taken into account in determining each flux term. For example, Q_t depends on not only the tidal condition but also the freshwater influx and discharge including the component induced by rainfall. Each term in equation (1) must be determined as a function of all forces. This applies to rainfall-induced Q_f, which can be influenced by the tidal condition as evident in the difference between Cases 2 and 5.

Two additional simulations (Cases 3 and 6) were conducted with the rainfall infiltration simulated indirectly by increasing the inland freshwater flux to account for the daily averaged infiltration rate. Both simulations produced similar results (supporting information Figure S1 and Table 1), which suggest that under both nontidal and tidal conditions, the long-term rainfall effect on nearshore groundwater (in terms of yearly averaged SGD and salt distribution) is determined largely by the amount of infiltration generated by rainfall.

3.2. Short-Term Effect of Episodic Rainfall Based on Daily Variations of SGD and SWI

The SGD and associated salt distribution varied temporally in response to alternating rain events and dry weather. These variations are expected to increase the variability of the nearshore groundwater system, which was previously examined in relation to tidal fluctuations [*Robinson et al.*, 2007a; *Xin et al.*, 2010]. The analysis presented here focused on the daily averaged results and aimed to determine how they were related to the episodic rainfall data.

The maximum daily average rainfall rate, 0.048 m/d, appeared on day 97 (Figure 2). However, the peak in the water efflux (SGD) occurred on day 101 for both Cases 2 (without tide) and Case 5 (with tide, Figure 5), i.e., the SGD response was delayed by 4 d. From day 101, an 8 d dry period started (Figure 2). However, the SGD in Cases 2 and 5 declined until day 110, when a small peak appeared (Figure 5). These results indicated that SGD responded to rainfall events in a delayed and prolonged fashion.

The rainfall effect also influenced the variations of daily averaged SM_{SW} (Figure 6). The trend was, however, opposite to that observed for the SGD. Figure 6b shows that in Case 5, SM_{SW} increased during days 118–150 while the SGD exhibited an overall decline (Figure 5). This inverse relationship is consistent with previous findings [*Kuan et al.*, 2012; *Michael et al.*, 2005]. An inhibiting effect of rainfall was evident in the
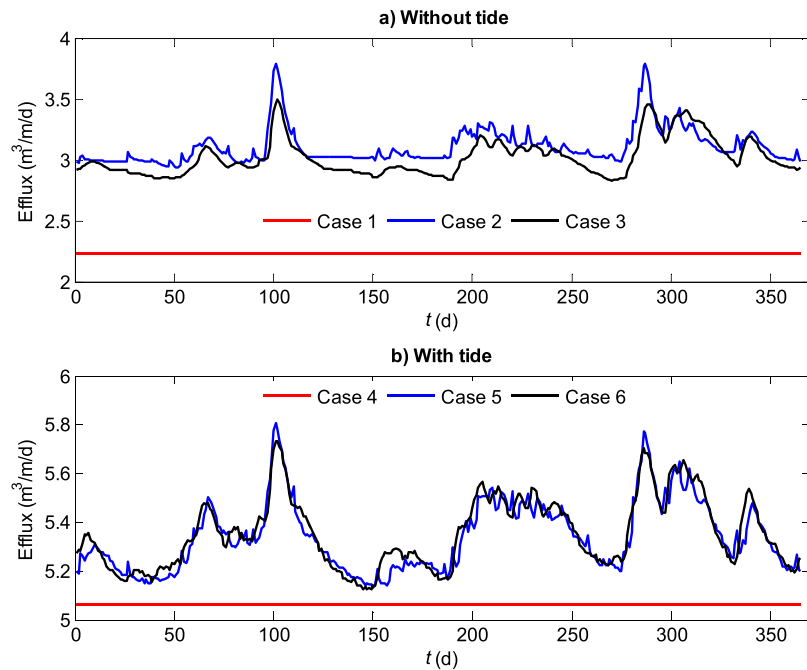
Figure 5. Daily averaged water efflux (SGD) across the per-unit-width aquifer-ocean interface.

variations of the SM_{USP} (Figures 7 and 8, Case 5). A nadir appeared on day 112 (Figure 7d), when the USP was at its shallowest position (Figures 7 and 8). With a similar amount of rainfall infiltration added directly to the inland boundary, Case 6 captured a similar SM_{USP} trend in comparison with Case 5 (Figure 8). This suggests that the salt mass stored in the USP (SM_{USP}) was mainly controlled by the inland freshwater input, rather than the dilution due to the rainfall-induced infiltration across the intertidal zone, which was small in comparison with the total infiltration into the aquifer platform.
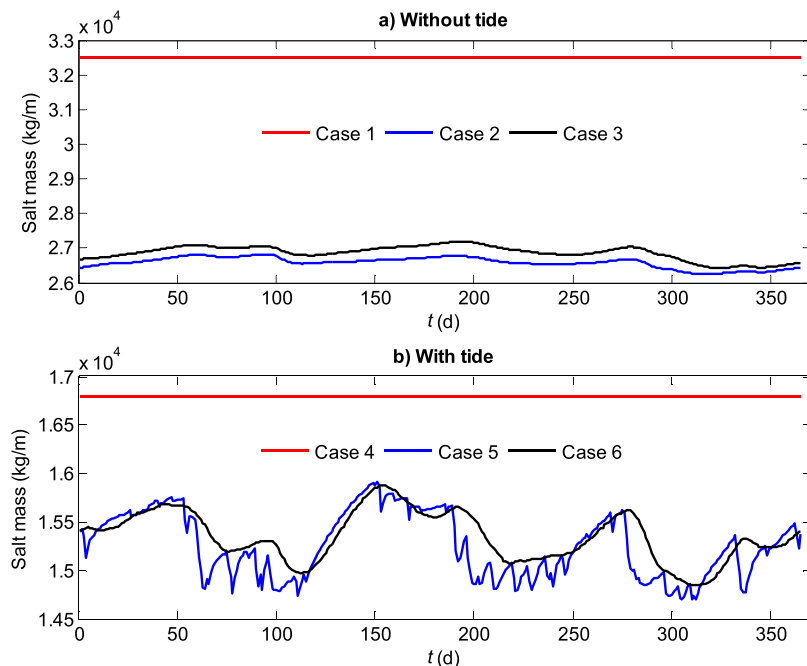

Figure 6. Daily averaged salt mass stored in the per-unit-width saltwater wedge.
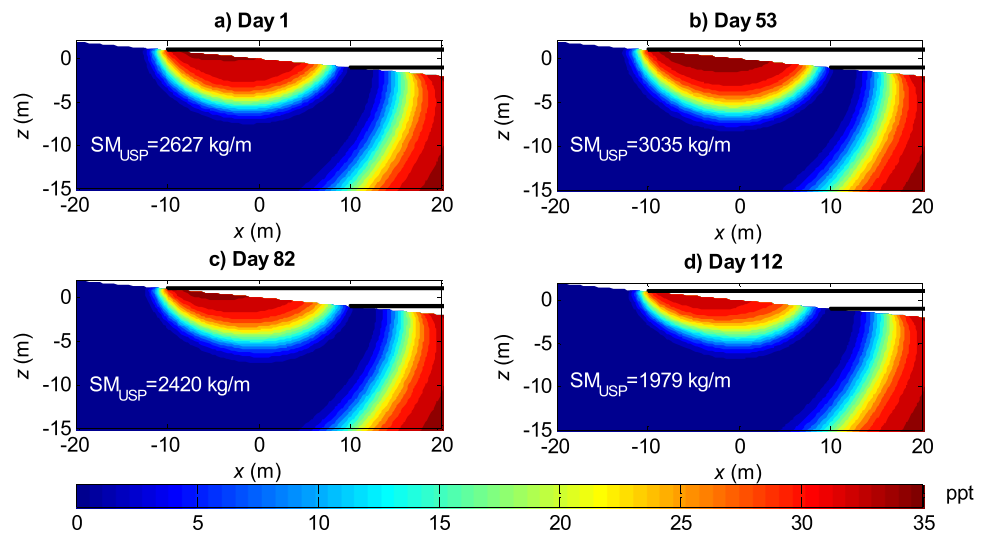
Figure 7. Snapshots of daily averaged salinity distributions for Case 5. The time is given in the figure titles and the salt mass stored in the per-unit-width upper saline plume is marked on the figure. Two black lines indicate the high and low tidal levels.

Simple regression models were found to be inadequate for describing the relationships of daily averaged SGD and salt storage with the daily average rainfall rate. We explored an approach based on functional data analysis (FDA), used in a wide range of research fields, including hydrology [*Ramsay and Silverman*, 2005; *Suhaila et al.*, 2011; *Wang et al.*, 2011; *Xin et al.*, 2014]. The effect of rainfall events was considered to follow a continuous and smooth function at the relevant (daily) temporal scale.

To quantify the prolonged and cumulative effect of (past) rainfall events, we hypothesized that these events can be weighted in the form of convolution:

$$DRI = \frac{\sum_{j=n}^{m} \zeta_j R_{t-j\Delta t}}{\sum_{j=n}^{m} \zeta_j} \tag{2}$$

where *DRI* is a parametric regressor, i.e., the weighted rainfall events combined in a cumulative fashion; t is the present time, $t - j\Delta t$ is the given past time with Δt being the increment (set to 1 d as the daily averaged results were used for the analysis), and $R_{t-j\Delta t}$ is the daily average rainfall at that time. The minimum and maximum values of j are, respectively, n and m, which define the past time period considered. ζ_j is a time-dependent weighting factor described by a Gamma distribution with the following probability density function (PDF):

$$\zeta_j \sim \text{Gamma}(\alpha, \beta, j\Delta t) = \beta^\alpha \frac{1}{\Gamma(\alpha)} (j\Delta t)^{\alpha-1} \exp(-\beta j\Delta t) \tag{3}$$

where α and β are, respectively, the shape and scale factors. The ratio α/β (i.e., the mean of the Gamma distribution PDF) controls the tail of the distribution and reflects the weight of past forcing conditions. It
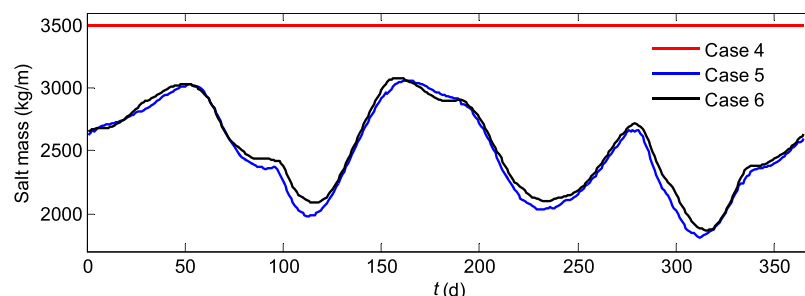

Figure 8. Daily averaged salt mass stored in the per-unit-width upper saline plume.

Table 2. Summary of Regression Results for Daily Averaged SGD and Salt Mass in SW and USP[a]

		Case 2	Case 3	Case 5	Case 6	Case 7	Case 8
SGD	α	1.50	2.00	1.76	1.50	2.40	1.6
	α/β	10.71	15.38	15.49	14.06	22.15	25.60
	Adjusted R^2	0.80	0.83	0.89	0.99	0.87	0.98
	a	87.91	63.32	64.12	65.16	72.10	67.66
	b	2.52	2.76	5.08	5.09	4.92	5.08
	Peak (d)	4	8	7	5	13	9
	MT (d)	22	30	31	29	42	53
SM_{SW}	α	1.62	1.80	1.20	3.80	1.20	3.52
	α/β	131.22	108.00	20.57	24.90	36.00	33.49
	Adjusted R^2	0.91	0.94	0.87	0.97	0.88	0.96
	a	-3.49×10^5	-4.04×10^5	-1.76×10^5	-1.34×10^5	-2.79×10^5	-1.31×10^5
	b	2.84×10^4	2.85×10^4	1.60×10^4	1.59×10^4	1.67×10^4	1.59×10^4
	Peak (d)	35	41	3	18	5	24
	MT (d)	224	197	46	42	79	58
SM_{USP}	α	NA	NA	3.10	3.30	3.60	3.52
	α/β	NA	NA	32.03	32.03	38.12	39.97
	Adjusted R^2	NA	NA	0.98	0.99	0.96	0.99
	a	NA	NA	-2.29×10^5	-2.13×10^5	-2.53×10^5	-2.03×10^5
	b	NA	NA	3.43×10^3	3.41×10^3	3.61×10^3	3.35×10^3
	Peak (d)	NA	NA	21	22	27	29
	MT (d)	NA	NA	56	56	66	70

[a]SGD is the submarine groundwater discharge; SM_{SW} is the salt mass stored in the saltwater wedge (per unit width aquifer); SM_{USP} is the salt mass stored in the upper saline plume; α and β are, respectively, the shape and scale factors of Gamma distribution function; a and b are the coefficients for the regression. Peak indicates the backward elapsed time for the maximum historic effect; MT is the memory time, i.e., the backward elapsed time for the rainfall effect to decay to 10%. NA means not applicable.

should be noted that we chose Gamma distribution function because it can be nonmonotonic (if $\alpha > 1$) and has the advantage of characterizing the delayed and prolonged effects of rainfall on SGD and SWI. With two parameters, it is widely used to describe flow and solute transport in various hydrological systems, e.g., for transit time modeling in catchment systems [*Kirchner et al.*, 2000; *McGuire and McDonnell*, 2006]. Furthermore, the Gamma distribution has no value at zero (i.e., required that $j\Delta t > 0$). In this study, we set n and m, respectively, to 1 and 365 (a year) and thus equation (2) does not consider the effect of the present rainfall event.

We then explored how daily averaged SGD, SM_{USP}, and SM_{SW} might be related to *DRI* based on a generalized linear model (GLM):

$$Y = aDRI + b \tag{4}$$

This regression model contains only four coefficients (α, β, a, and b), which assists in assessing the effect of rainfall on the considered subterranean estuary.

This model (equation (4)) fitted the simulated results well (summarized in Table 2). For Case 2 without the tide, the slope of the regression (a) of equation (4) was positive (87.91 m) for the SGD but negative (-3.49×10^5 kgd/m^2) for the SM_{SW}, which is consistent with the overall effect that rainfall increased the SGD but inhibited the SWI. The two fitted Gamma distribution PDFs were nonmonotonic with $\alpha > 1$, suggesting that the past rainfall effect did not decay immediately (Figure 9 and Table 2). For the SGD, the peak of the fitted PDF appeared on day 4, corresponding with the occurrence of the maximum rainfall effect. We further calculated the backward elapsed time when the rainfall effect decayed to 10% (defined as memory time, MT) based on the fitted PDF. For Case 2, the MT for the SGD was 22 d, suggesting that the present SGD was still affected considerably by rainfall events 22 d before. The past rainfall effect on SM_{SW} was more long-lasting. The peak occurred on day 35 with MT = 224 d. A similarly strong past rainfall effect was found for Case 3 (in which the equivalent rainfall infiltration was added to the inland boundary, Table 2 and supporting information Figure S2). The peak occurred on day 41 with MT = 197 d.

In the tidally influenced aquifer, the SGD and SWI were also significantly affected by past rainfall events (Case 5, Figure 10 and Table 2). While the MT for the SGD differed little from the nontidal case, the MT for the SM_{SW} was dramatically reduced from 224 (Case 2) to 46 (Case 5) d under the tidal influence (Table 2). This shows the competition between tides and rainfall infiltration in affecting SWI. The tidal effect weakened the influence of past rainfall and hence shortened its MT. For SM_{USP}, both the peak (day 21) and MT (56 d)
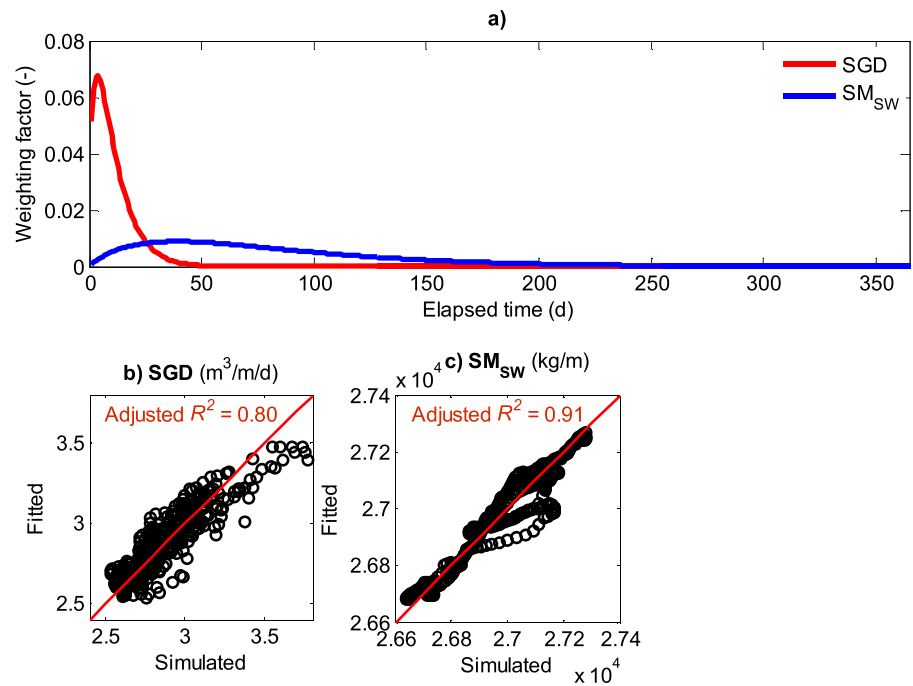
Figure 9. (a) Gamma distribution functions used for quantifying the effect of past rainfall events on the subterranean estuary (Case 2); (b and c) Fitted results versus those simulated.

were longer than those for SM_{SW} (day 3 and 46 d, respectively). This suggests that the effect of (past) rainfall on USP lasted longer than that on SW. This behavior is also evident in the comparison between Cases 5 and 6 (Figure 10 and supporting information Figure S3). With the equivalent rainfall infiltration rate added to the inland boundary, Case 6 simulated well the rainfall effect on USP with the regression model for SM_{USP} close to that of Case 5 (Table 2).
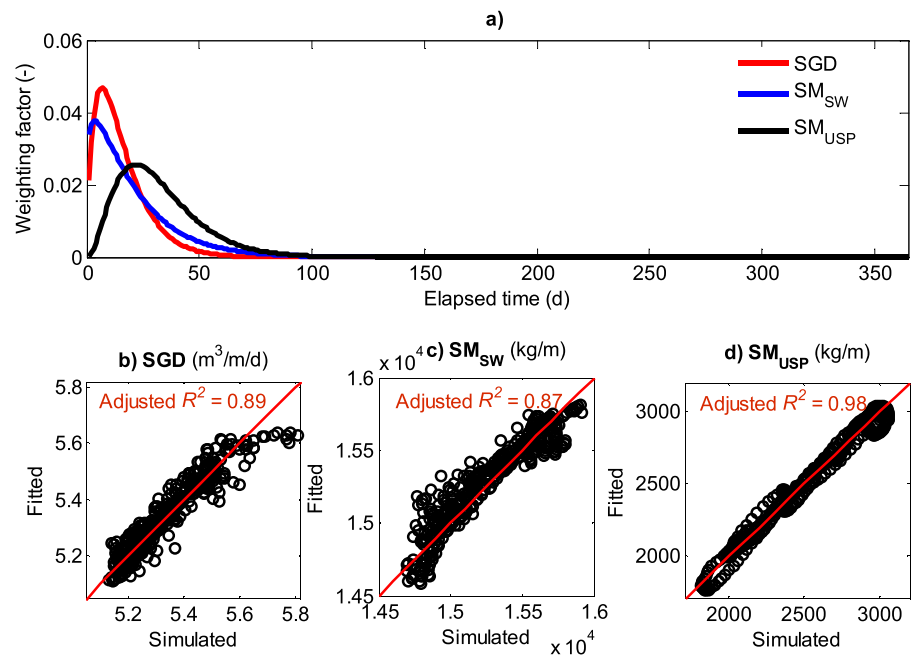

Figure 10. (a) Gamma distribution functions used for quantifying the effect of past rainfall events on the subterranean estuary (Case 5); (b–d) Fitted results versus those simulated.
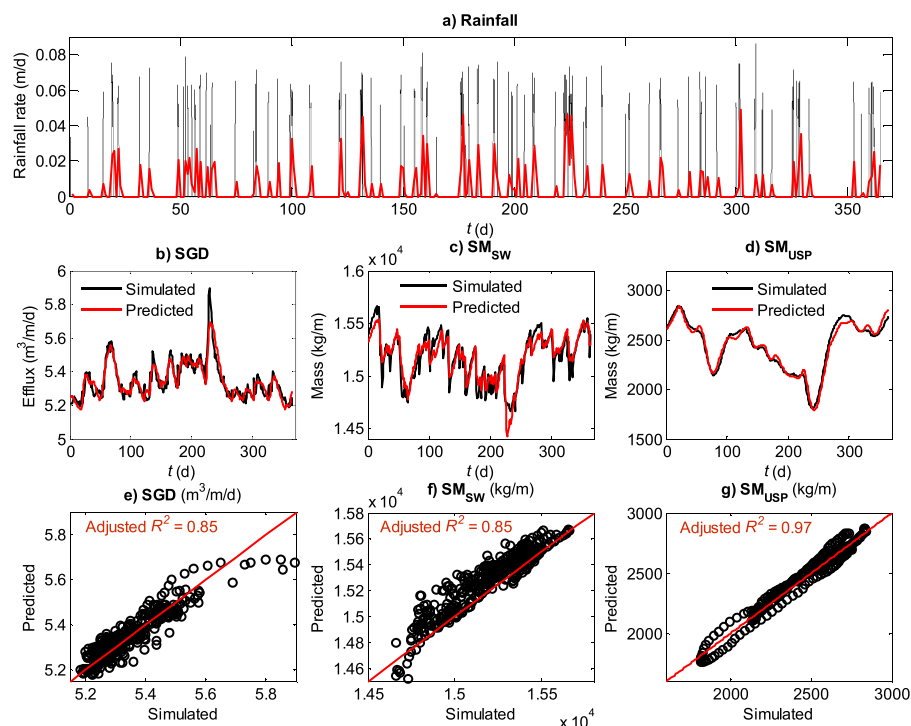
Figure 11. (a) Annual rainfall time series used for the prediction (series generated using the Markov-chain Monte-Carlo simulator with the same statistical parameters as the rainfall time series in Figure 2). The red line indicates the daily averaged results. (b–d) Daily averaged SGD, SM$_{SW}$, and SM$_{USP}$ predicted by the regression model in comparison with the simulated results (Case 5). (e–g) Predicted results versus those simulated.

The GLM is essentially a memory-dependent linear signal filter. Despite the simplicity, it appears to capture the characteristics of episodic rainfall effects on the different metrics of the simulated subterranean estuary since all the adjusted R^2 values are larger than 0.8 (Table 2).

3.3. Predictability of the SGD and SWI Affected by Episodic Rainfall

We next consider if the GLM given by equation (4) captures the behavior of the nearshore aquifer when subjected to rainfall of different patterns. For this purpose, we generated another yearlong rainfall series using the Markov-chain Monte-Carlo simulator with the same statistical parameters (Figure 11a). We continued to run the SUTRA simulations for the four cases with rainfall considered, i.e., using the results at the end of the year (day 365) as the initial conditions of the new simulations. The GLM, derived from previous simulations based on the rainfall data set in Figure 2, satisfactorily predicted the newly simulated SGD, SM$_{SW}$, and SM$_{USP}$ averaged over a daily cycle (Figure 11 and supporting information Figures S4–S6). The model performed even better for the tidal case (Figure 11, Case 5). For the SM$_{USP}$, the simulated and predicted results largely overlap with adjusted R^2 up to 0.97 (Figures 11d and 11g).

3.4. Influence of Model Domain

With the model domain extended in either the upward (Case 7) or landward (Case 8) directions, the yearly averaged SGD, SM$_{SW}$, and SM$_{USP}$ did not change considerably (Table 1). This suggests that the total freshwater input controlled the overall long-term behavior of the nearshore aquifer system. However, the responses of the daily averaged SGD, SM$_{SW}$, and SM$_{USP}$ were further delayed as indicated by postponed peaks of the fitted PDFs for daily averaged SGD, SM$_{SW}$, and SM$_{USP}$ curves (supporting information Figures S7–S9). As expected, the travel time of the freshwater increased for both the aquifer with a thickened vadose zone (Case 7) and that with the landward boundary moved inland (Case 8). The prolonged effects of rainfall were well quantified by the regression model (supporting information Figures S10–S12). Both the peak time (time for the maximum historic effect) and MT (time for the rainfall effect to decay to 10%) given by the PDFs increased (Table 2). For example, the peak time increased from 7 d for Case 5 to 13 d for Case 7, while

MT increased from 31 to 42 d. These increases are consistent with the theory of groundwater wave propagation in unconfined aquifers [*Li et al.*, 1997, 2000; *Nielsen*, 2009; *Parlange et al.*, 1984].

4. Discussion and Concluding Remarks

Rainfall generates freshwater influx to coastal aquifers, which subsequently discharges to the sea. As rainfall events are episodic, this influx tends to be highly variable. However, most previous modeling studies incorporated the freshwater input via the inland boundary of the aquifer with a fixed flux or head, overlooking the variability and randomness of natural systems [*Lu et al.*, 2015; *Michael et al.*, 2013; *Werner et al.*, 2013]. This paper quantified the SGD and SWI processes in a nearshore aquifer subjected to the influence of episodic rainfall, and uncovered the delayed and prolonged rainfall effect. The findings have the following implications for future investigations on coastal and offshore environments:

1. Different forces on the nearshore groundwater system interact strongly. While simple models such as equation (1) may still be applicable for predictions of SGD, each term attributed to a particular force must be determined with consideration of the influence of other forces.
2. The interactions of the forces also affect the short-term behavior of the nearshore groundwater. Tides appear to shorten the period of past rainfall influence on nearshore groundwater dynamics, particularly seawater circulations through the USP and SW.
3. The rainfall effect coupled with the influence of other forces must be considered in the studies of coastal groundwater dynamics. In particular, field investigations need to account for the effect of past rainfall events during both data collection and analysis.
4. Meteorological data including rainfall are available widely in coastal zones around the world. Combined with data of other forcing factors such as tides and waves, these meteorological data allow the development of FDA models for predicting SGD and associated solute fluxes worldwide. These predictive models have a simple form and would be of direct use in developing strategies for protection of nearshore environments and groundwater resources management.

While the present study has generated insights into the SGD and SWI in a nearshore aquifer subjected to the influence of episodic rainfall, further investigations are needed to explore the following aspects:

1. Soil hydraulic conductivity, capillarity, and beach slope are key aquifer properties and worthy of detailed studies, particularly to explore how these parameters modify the coefficients of the generalized linear model. The model domain was a 2-D vertical section perpendicular to the shoreline, and the aquifer was homogeneous and isotropic. Heterogeneous aquifer properties should be investigated. Three-dimensionality linked strongly to the beach morphology and land surface topography is likely to alter the SGD and SWI [*Zhang et al.*, 2016]. Local topographic variations, rather than the idealized geometry used here, are expected to affect rainfall infiltration and groundwater flow in both cross-shore and along-shore directions.
2. Wave forcing and multiple tidal constituents (e.g., combined semidiurnal solar and lunar tides) were not considered. These factors would provide additional forcing on the flow and associated solute transport in a nearshore aquifer. Particularly, wave motions are highly variable. It remains to be determined how this variability combined with episodic rainfall events would be manifested in the SGD and SWI.
3. Variations of SGD and SWI over the tidal cycle are significantly altered by tidal fluctuations. While we have quantified the daily variation of SGD and SWI, an improved statistical model with high-order terms is needed to unravel the intratidal variations of SGD and SWI.

Although these research questions remain unsolved, the generalized linear model developed based on functional data analysis is a potentially useful approach to characterizing and quantifying the complex SGD and SWI processes in a nearshore aquifer, subjected to irregular forcing factors such as rainfall.

References

Anschutz, P., T. Smith, A. Mouret, J. Deborde, S. Bujan, D. Poirier, and P. Lecroart (2009), Tidal sands as biogeochemical reactors, *Estuarine Coastal Shelf Sci.*, *84*(1), 84–90, doi:10.1016/j.ecss.2009.06.015.

Bakhtyar, R., D. A. Barry, and A. Brovelli (2012), Numerical experiments on interactions between wave motion and variable-density coastal aquifers, *Coastal Eng.*, *60*, 95–108, doi:10.1016/j.coastaleng.2011.09.001.

Bakhtyar, R., A. Brovelli, D. A. Barry, C. Robinson, and L. Li (2013), Transport of variable-density solute plumes in beach aquifers in response to oceanic forcing, *Adv. Water Resour.*, *53*, 208–224, doi:10.1016/j.advwatres.2012.11.009.

Boufadel, M. C. (2000), A mechanistic study of nonlinear solute transport in a groundwater-surface water system under steady state and transient hydraulic conditions, *Water Resour. Res.*, *36*(9), 2549–2565, doi:10.1029/2000WR900159.

Brovelli, A., X. Mao, and D. A. Barry (2007), Numerical modeling of tidal influence on density-dependent contaminant transport, *Water Resour. Res.*, *43*, W10426, doi:10.1029/2006WR005173.

Burnett, W. C., et al. (2006), Quantifying submarine groundwater discharge in the coastal zone via multiple methods, *Sci. Total Environ.*, *367*(2–3), 498–543, doi:10.1016/j.scitotenv.2006.05.009.

Carsel, R. F., and R. S. Parrish (1988), Developing joint probability distributions of soil water retention characteristics, *Water Resour. Res.*, *24*(5), 755–769, doi:10.1029/WR024i005p00755.

Cooper, H. H. (1959), A hypothesis concerning the dynamic balance of fresh water and salt water in a coastal aquifer, *J. Geophys. Res.*, *64*(4), 461–467, doi:10.1029/JZ064i004p00461.

Evans, T. B., and A. M. Wilson (2016), Groundwater transport and the freshwater-saltwater interface below sandy beaches, *J. Hydrol.*, *538*, 563–573, doi:10.1016/j.jhydro1.2016.04.014.

Evans, T. B., and A. M. Wilson (2017), Submarine groundwater discharge and solute transport under a transgressive barrier island, *J. Hydrol.*, *574*, 97–110, doi:10.1016/j.jhydrol.2017.01.028.

Geng, X., and M. C. Boufadel (2015), Impacts of evaporation on subsurface flow and salt accumulation in a tidally influenced beach, *Water Resour. Res.*, *51*, 5547–5565, doi:10.1002/2015WR016886.

Geng, X., M. C. Boufadel, Y. Xia, H. Li, L. Zhao, N. L. Jackson, and R. S. Miller (2014), Numerical study of wave effects on groundwater flow and solute transport in a laboratory beach, *J. Contam. Hydrol.*, *165*, 37–52, doi:10.1016/j.jconhyd.2014.07.001.

Geng, X. L., M. C. Boufadel, and N. L. Jackson (2016), Evidence of salt accumulation in beach intertidal zone due to evaporation, *Sci. Rep.*, *6*, 31,486, doi:10.1038/srep31486.

Glover, R. (1959), The pattern of fresh-water flow in a coastal aquifer, *J. Geophys. Res.*, *64*(4), 457–459, doi:10.1029/JZ064i004p00457.

Heiss, J. W., and H. A. Michael (2014), Saltwater-freshwater mixing dynamics in a sandy beach aquifer over tidal, spring-neap, and seasonal cycles, *Water Resour. Res.*, *50*, 6747–6766, doi:10.1002/2014WR015574.

Heiss, J. W., J. A. Puleo, W. J. Ullman, and H. A. Michael (2015), Coupled surface-subsurface hydrologic measurements reveal infiltration, recharge, and discharge dynamics across the swash zone of a sandy beach, *Water Resour. Res.*, *51*, 8834–8853 doi:10.1002/2015WR017395.

Jun, S. C., G. O. Bae, and K. K. Lee (2013), Factors causing dynamic variations in the saltwater-freshwater transition zone in a beach aquifer, Mangsang, South Korea, *Hydrogeol. J.*, *21*(6), 1355–1371, doi:10.1007/s10040-013-0995-y.

King, J. N. (2012), Synthesis of benthic flux components in the Patos Lagoon coastal zone, Rio Grande do Sul, Brazil, *Water Resour. Res.*, *48*, W12530, doi:10.1029/2011WR011477.

Kirchner, J. W., X. H. Feng, and C. Neal (2000), Fractal stream chemistry and its implications for contaminant transport in catchments, *Nature*, *403*(6769), 524–527, doi:10.1038/35000537.

Kuan, W. K., G. Q. Jin, P. Xin, C. Robinson, B. Gibbes, and L. Li (2012), Tidal influence on seawater intrusion in unconfined coastal aquifers, *Water Resour. Res.*, *48*, W02502, doi:10.1029/2011WR010678.

Kwon, E. Y., G. Kim, F. Primeau, W. S. Moore, H. M. Cho, T. DeVries, J. L. Sarmiento, M. A. Charette, and Y. K. Cho (2014), Global estimate of submarine groundwater discharge based on an observationally constrained radium isotope model, *Geophys. Res. Lett.*, *41*, 8438–8444, doi:10.1002/2014GL061574.

Li, L., and D. A. Barry (2000), Wave-induced beach groundwater flow, *Adv. Water Resour.*, *23*(4), 325–337, doi:10.1016/s0309-1708(99)00032-9.

Li, L., D. Barry, and C. Pattiaratchi (1997), Numerical modelling of tide-induced beach water table fluctuations, *Coastal Eng.*, *30*(1), 105–123, doi:10.1016/S0378-3839(96)00038-5.

Li, L., D. A. Barry, F. Stagnitti, and J.-Y. Parlange (1999), Submarine groundwater discharge and associated chemical input to a coastal sea, *Water Resour. Res.*, *35*(11), 3253–3259, doi:10.1029/1999WR900189.

Li, L., D. A. Barry, F. Stagnitti, J.-Y. Parlange, and D. S. Jeng (2000), Beach water table fluctuations due to spring-neap tides: Moving boundary effects, *Adv. Water Resour.*, *23*(8), 817–824, doi:10.1016/s0309-1708(00)00017-8.

Li, H., M. C. Boufadel, and J. W. Weaver (2008), Tide-induced seawater-groundwater circulation in shallow beach aquifers, *J. Hydrol.*, *352*(1–2), 211–224, doi:10.1016/j.jhydrol.2008.01.013.

Li, X. Y., B. X. Hu, W. C. Burnett, I. R. Santos, and J. P. Chanton (2009), Submarine ground water discharge driven by tidal pumping in a heterogeneous aquifer, *Ground Water*, *47*(4), 558–568, 10.1111/j.1745-6584.2009.00563.x.

Liu, Y., J. J. Jiao, and X. Luo (2016), Effects of inland water level oscillation on groundwater dynamics and land-sourced solute transport in a coastal aquifer, *Coastal Eng.*, *114*, 347–360, doi:10.1016/j.coastaleng.2016.04.021.

Longuet-Higgins, M. S. (1983), Wave set-up, percolation and undertow in the surf zone, *Proc. R. Soc. London, Ser. A*, *390*(1799), 283–291, doi:10.1098/rspa.1983.0132.

Lu, C., P. Xin, L. Li, and J. Luo (2015), Seawater intrusion in response to sea-level rise in a coastal aquifer with a general-head inland boundary, *J. Hydrol.*, *522*, 135–140, doi:10.1016/j.jhydrol.2014.12.053.

Mao, X., P. Enot, D. A. Barry, L. Li, A. Binley, and D. S. Jeng (2006), Tidal influence on behaviour of a coastal aquifer adjacent to a low-relief estuary, *J. Hydrol.*, *327*(1–2), 110–127, doi:10.1016/j.jhydrol.2005.11.030.

McGuire, K. J., and J. J. McDonnell (2006), A review and evaluation of catchment transit time modeling, *J. Hydrol.*, *330*(3–4), 543–563, doi:10.1016/j.jhydrol.2006.04.020.

Michael, H. A., A. E. Mulligan, and C. F. Harvey (2005), Seasonal oscillations in water exchange between aquifers and the coastal ocean, *Nature*, *436*(7054), 1145–1148, doi:10.1038/nature03935.

Michael, H. A., C. J. Russoniello, and L. A. Byron (2013), Global assessment of vulnerability to sea-level rise in topography-limited and recharge-limited coastal groundwater systems, *Water Resour. Res.*, *49*, 2228–2240, doi:10.1002/wrcr.20213.

Michael, H. A., K. C. Scott, M. Koneshloo, X. Yu, M. R. Khan, and K. Li (2016), Geologic influence on groundwater salinity drives large seawater circulation through the continental shelf, *Geophys. Res. Lett.*, *43*, 10,782–10,791, doi:10.1002/2016GL070863.

Moore, W. S. (1996), Large groundwater inputs to coastal waters revealed by Ra-226 enrichments, *Nature*, *380*(6575), 612–614, doi:10.1038/380612a0.

Moore, W. S. (1999), The subterranean estuary: A reaction zone of ground water and sea water, *Mar. Chem.*, *65*(1–2), 111–125, doi:10.1016/s0304-4203(99)00014-6.

Moore, W. S. (2010), The effect of submarine groundwater discharge on the ocean, *Annu. Rev. Mar. Sci.*, *2*, 59–88, doi:10.1146/annurev-marine-120308-081019.

Moore, W. S., J. L. Sarmiento, and R. M. Key (2008), Submarine groundwater discharge revealed by Ra-228 distribution in the upper Atlantic Ocean, *Nat. Geosci.*, *1*(5), 309–311, doi:10.1038/ngeo183.

Morris, J. T. (1995), The mass balance of salt and water in intertidal sediments: Results from North Inlet, South Carolina, *Estuaries*, *18*(4), 556–567, doi:10.2307/1352376.

Nielsen, P. (2009), *Coastal and Estuarine Processes*, World Scientific, Singapore.

Parlange, J.-Y., F. Stagnitti, J. Starr, and R. Braddock (1984), Free-surface flow in porous media and periodic solution of the shallow-flow approximation, *J. Hydrol.*, *70*(1), 251–263, doi:10.1016/0022-1694(84)90125-2.

Ramsay, J. O., and B. W. Silverman (2005), *Functional Data Analysis*, Springer, New York.

Richards, L. A. (1931), Capillary conduction of liquids through porous mediums, *Physics*, *1*(5), 318–333.

Robinson, C., B. Gibbes, and L. Li (2006), Driving mechanisms for groundwater flow and salt transport in a subterranean estuary, *Geophys. Res. Lett.*, *33*, L03402, doi:10.1029/2005GL025247.

Robinson, C., L. Li, and D. A. Barry (2007a), Effect of tidal forcing on a subterranean estuary, *Adv. Water Resour.*, *30*(4), 851–865, doi:10.1016/j.advwatres.2006.07.006.

Robinson, C., L. Li, and H. Prommer (2007b), Tide-induced recirculation across the aquifer-ocean interface, *Water Resour. Res.*, *43*, W07428, doi:10.1029/2006WR005679.

Robinson, C., A. Brovelli, D. A. Barry, and L. Li (2009), Tidal influence on BTEX biodegradation in sandy coastal aquifers, *Adv. Water Resour.*, *32*(1), 16–28, doi:10.1016/j.advwatres.2008.09.008.

Robinson, C., P. Xin, L. Li, and D. A. Barry (2014), Groundwater flow and salt transport in a subterranean estuary driven by intensified wave conditions, *Water Resour. Res.*, *50*, 165–181, doi:10.1002/2013WR013813.

Rodellas, V., J. Garcia-Orellana, P. Masqué, M. Feldman, and Y. Weinstein (2015), Submarine groundwater discharge as a major source of nutrients to the Mediterranean Sea, *Proc. Natl. Acad. Sci. U. S. A.*, *112*(13), 3926–3930, doi:10.1073/pnas.1419049112.

Santos, I. R., B. D. Eyre, and M. Huettel (2012), The driving forces of porewater and groundwater flow in permeable coastal sediments: A review, *Estuarine Coastal Shelf Sci.*, *98*, 1–15, doi:10.1016/j.ecss.2011.10.024.

Sawyer, A. H., F. Shi, J. T. Kirby, and H. A. Michael (2013), Dynamic response of surface water-groundwater exchange to currents, tides, and waves in a shallow estuary, *J. Geophys. Res. Oceans*, *118*, 1749–1758, doi:10.1002/jgrc.20154.

Smith, A. J. (2004), Mixed convection and density-dependent seawater circulation in coastal aquifers, *Water Resour. Res.*, *40*, W08309, doi:10.1029/2003WR002977.

Suhaila, J., A. A. Jemain, M. F. Hamdan, and W. Z. W. Zin (2011), Comparing rainfall patterns between regions in Peninsular Malaysia via a functional data analysis technique, *J. Hydrol.*, *411*(3–4), 197–206, doi:10.1016/j.jhydrol.2011.09.043.

Taniguchi, M., W. C. Burnett, J. E. Cable, and J. V. Turner (2002), Investigation of submarine groundwater discharge, *Hydrol. Processes*, *16*(11), 2115–2129, doi:10.1002/hyp.1145.

van-Genuchten, M. T. (1980), A closed-form equation for predicting the hydraulic conductivity of unsaturated soils, *Soil Sci. Soc. Am. J.*, *44*(5), 892–898.

Voss, C. I., and A. M. Provost (2008), A Model for Saturated-Unsaturated, Variable-Density Ground-Water Flow with Solute or Energy Transport, U.S. Geol. Surv., Reston, Va.

Wang, Y. G., P. Kuhnert, and B. Henderson (2011), Load estimation with uncertainties from opportunistic sampling data—A semiparametric approach, *J. Hydrol.*, *396*(1–2), 148–157, doi:10.1016/j.jhydrol.2010.11.003.

Wang, X., H. Li, J. J. Jiao, D. Barry, L. Li, X. Luo, C. Wang, L. Wan, X. Wang, and X. Jiang (2015), Submarine fresh groundwater discharge into Laizhou Bay comparable to the Yellow River flux, *Sci. Rep.*, *5*, 8814, doi:10.1038/srep08814.

Werner, A. D., M. Bakker, V. E. Post, A. Vandenbohede, C. Lu, B. Ataie-Ashtiani, C. T. Simmons, and D. A. Barry (2013), Seawater intrusion processes, investigation and management: Recent advances and future challenges, *Adv. Water Resour.*, *51*, 3–26, doi:10.1016/j.advwatres.2012.03.004.

Wilson, A. M., T. B. Evans, W. S. Moore, C. A. Schutte, and S. B. Joye (2015), What time scales are important for monitoring tidally influenced submarine groundwater discharge? Insights from a salt marsh, *Water Resour. Res.*, *51*, 4198–4207, doi:10.1002/2014WR015984.

Xin, P., C. Robinson, L. Li, D. A. Barry, and R. Bakhtyar (2010), Effects of wave forcing on a subterranean estuary, *Water Resour. Res.*, *46*, W12505, doi:10.1029/2010WR009632.

Xin, P., S. S. J. Wang, C. Robinson, L. Li, Y.-G. Wang, and D. A. Barry (2014), Memory of past random wave conditions in submarine groundwater discharge, *Geophys. Res. Lett.*, *41*, 2401–2410, doi:10.1002/2014GL059617.

Xin, P., S. S. J. Wang, C. Lu, C. Robinson, and L. Li (2015), Nonlinear interactions of waves and tides in a subterranean estuary, *Geophys. Res. Lett.*, *42*, 2277–2284, doi:10.1002/2015GL063643.

Zhang, Y., L. Li, D. V. Erler, I. Santos, and D. Lockington (2016), Effects of alongshore morphology on groundwater flow and solute transport in a nearshore aquifer, *Water Resour. Res.*, *52*, 990–1008, doi:10.1002/2015WR017420.